2004

Numerical Study of the Diapycnal Flow Through a Tidal Front With Passive Tracers

Chingming Dong

Robert Houghton

Hsien-Wang Ou

Dake Chen

Tal Ezer
Old Dominion University, tezer@odu.edu

Original Publication Citation

Dong, C., Houghton, R., Ou, H.W., Chen, D., & Ezer, T. (2004). Numerical study of the diapycnal flow through a tidal front with passive tracers. *Journal of Geophysical Research C: Oceans, 109*(5), 1-13. doi: 10.1029/2003JC001969

Numerical study of the diapycnal flow through a tidal front with passive tracers

Changming Dong
Institute of Geophysics and Planetary Physics, University of California, Los Angeles, California, USA

Robert Houghton, Hsien-Wang Ou, and Dake Chen
Lamont-Doherty Earth Observatory, Columbia University, Palisades, New York, USA

Tal Ezer
Program in Atmospheric and Oceanic Sciences, Princeton University, Princeton, New Jersey, USA

Received 20 May 2003; revised 3 March 2004; accepted 8 April 2004; published 26 May 2004.

[1] A two-dimensional numerical model is used to study the diapycnal flow through a tidal front with passive tracers. In a basic numerical experiment a passive tracer is released into the bottom water at the offshore edge of a tidal front, and it subsequently moves on-bank with a velocity that decreases with time. This qualitatively agrees with a recent field experiment using a dye tracer on Georges Bank. Additional experiments are performed to investigate the sensitivity of the tracer dispersion to the tidal phase and the location of tracer release within the front. As the release point is moved on-bank across the front, the tracer velocity decreases until it weakly reverses on the on-bank edge of the front. This trend can be understood by considering the structure of the Lagrangian velocity field in the tidal front, the degree of vertical mixing of the tracer, and the concentration-weighted mean patch velocity. The tidal phase at the time of tracer release does not significantly affect the tracer dispersion. *INDEX TERMS:* 4546 Oceanography: Physical: Nearshore processes; 4255 Oceanography: General: Numerical modeling; 4568 Oceanography: Physical: Turbulence, diffusion, and mixing processes; 4560 Oceanography: Physical: Surface waves and tides (1255); *KEYWORDS:* passive tracer, diapycnal flow, tidal front

Citation: Dong, C., R. Houghton, H.-W. Ou, D. Chen, and T. Ezer (2004), Numerical study of the diapycnal flow through a tidal front with passive tracers, *J. Geophys. Res.*, *109*, C05029, doi:10.1029/2003JC001969.

1. Introduction

[2] Last two decades have witnessed numerous investigations of the circulation associated with tidally mixed fronts. The along-front component, dominated by the thermal-wind shear and tidal rectification, has well been studied by theoretical and modeling studies [*Loder*, 1980; *Garrett and Loder*, 1981; *Loder and Wright*, 1985; *Naimie et al.*, 1994; *Naimie*, 1996; *Lynch et al.*, 1996; *Chen and Beardsley*, 1998; *Ou*, 1999, 2000; *Chen et al.*, 2003] and field observations [*Butman and Beardsley*, 1987; *Loder and Brickman*, 1992; *Loder et al.*, 1993; *Limeburner and Beardsley*, 1996]. In contrast, due in part to its much weaker magnitude (1–3 cm/s, one order smaller than the along-shore flow), the cross-front component is less well understood and more complicated. For example, the previous studies indicated Eulerian cross-front mean circulation maybe is in a multiple-cell structure [*Loder and Wright*, 1985; *Chen and Beardsley*, 1998; *Dong et al.*, 2004; C. Dong et al., Tidally induced cross-front mean circulation: Numerical study, submitted to *Journal of Physical Oceanography*, 2003, hereinafter referred to as Dong et al., submitted manuscript, 2003].

[3] Direct Eulerian measurements of mean cross-front flow is difficult because tidal velocity is more than an order larger than the mean flow in magnitude, resulting in large excursions of the front. To overcome these difficulties, a dye patch, acting as a passive tracer, was used to measure the Lagrangian cross-front flow [*Houghton and Ho*, 2001; *Houghton*, 2002]. The experiments were conducted in the summer of 1999 over Georges Bank. The diapycnal velocities of the dye patch (on-bank) in the bottom mixed layer ranged from 4 cm/s on the northeast peak to 2 cm/s on the south flank.

[4] The on-bank near-bottom Lagrangian residual flow was first described by *Loder et al.* [1997]. Through tracking fluid particles in a tidal-driven three-dimensional homogenous flow field, they found that the Stokes' drift contribution was similar in magnitude to the Eulerian residual flow, leading to on-bank water movement near the bottom. *Chen and Beardsley* [1998] simulated the on-bank Lagrangian velocity of fluid particles and the on-bank transport of a passive tracer patch in a two-dimensional model. They examined the effect of vertical mixing on a tracer and suggested that the vertical mixing enhanced the net up-slope advection

0148-0227/04/2003JC001969

with a tracer initially occupying the water volume below a certain water depth. Applying three-dimensional model, *Chen et al.* [2003] further studied the cross-frontal water exchange. Using bimonthly climatological forcing, *Naimie et al.* [2001] compared the drifter trajectories simulated by Dartmouth circulation model with satellite-tracked drifters.

[5] In the present paper, rather than conducting a realistic simulation of the dye experiment over Georges Bank, we use a two-dimensional model (cross-shore section) to study the dispersion of a passive tracer patch in a tidal front. Applying a two-dimensional model in the study is encouraged by the favorable comparison of two-dimensional model experiments by *Chen and Beardsley* [1998] with three-dimensional model experiments [*Naimie et al.*, 1994, 2001; *Naimie*, 1996; *Chen et al.*, 2001, 2003]. The application of a two-dimensional model in the southern flank of Georges Bank is also justified by a scale analysis.

[6] We perform a basic numerical experiment using a tracer patch whose size is initially comparable with that of the field experiment, in which the initial dye streak was about 500 m in length. A series of tracer experiments are conducted to assess the sensitivity of the tracer dispersion to release positions and tidal phases in order to obtain a systematic view of the diapycnal flow through a tidal front. With a calculated Lagrangian velocity field we try to better understand what the movement of the tracer patch in the above field experiment represents? Intuitively, it represents the movement of the tagged water mass, i.e., the Lagrangian flow at the release point. At the initial stage, when the scale of the tracer is less than that of the velocity variation, the intuition is correct. When the tracer disperses and its scale exceeds the spatial scale of the velocity variation, the patch cannot be considered as a single point any more because the fluid parcels involved have different velocities, and the tracer patch movement is due to the ensemble velocity of all the fluid parcels involved.

[7] The paper is organized as follows. Section 2 is the scale analysis. Section 3 is the numerical experiments. In section 4, model results are compared with the field dye experiment. In section 5, tracer movement is compared with the model derived Lagrangian velocity field. Sections 6 and 7 are discussion and conclusions, respectively.

2. Scale Analysis

[8] With the hydrostatic and Boussinesq approximations, the three-dimensional governing equations are

$$\frac{\partial u^*}{\partial t^*}+u^*\frac{\partial u^*}{\partial x^*}+v^*\frac{\partial u^*}{\partial y^*}+w^*\frac{\partial u^*}{\partial z^*}-fv^*=-\frac{1}{\rho_0}\frac{\partial p^*}{\partial x^*}+\upsilon\frac{\partial^2 u^*}{\partial z^{*2}}, \tag{1}$$

$$\frac{\partial v^*}{\partial t^*}+u^*\frac{\partial v^*}{\partial x^*}+v^*\frac{\partial v^*}{\partial y^*}+w^*\frac{\partial v^*}{\partial z^*}+fu^*=-\frac{1}{\rho_0}\frac{\partial p^*}{\partial y^*}+\nu\frac{\partial^2 v^*}{\partial z^{*2}}, \tag{2}$$

$$\frac{\partial u^*}{\partial x^*}+\frac{\partial v^*}{\partial y^*}+\frac{\partial w^*}{\partial z^*}=0, \tag{3}$$

$$\frac{\partial p^*}{\partial z^*}=-\rho^* g, \tag{4}$$

where the x axis is perpendicular to the isobaths in the direction of increasing depth, the y axis is oriented with the shallow area to its left, and the z axis increases upward from the sea surface, g is the gravitational acceleration, t is the time, F is the Coriolis coefficient, ν is the vertical eddy diffusivity coefficient. p is the pressure, ρ_0 is the reference density, and (u, v, w) are the velocity components. Asterisks (*) represent dimensional parameters while a variable with no asterisk is dimensionless except for these parameters: f, g, k and ν. Variables can be decomposed into the time mean (overbar) and tidal variables (prime):

$$\begin{aligned}(u^*, v^*, w^*, p^*, \rho^*)&\\ =(\bar{u}^*+u'^*, \bar{v}^*+v'^*, \bar{w}^*+w'^*, \bar{p}^*+p'^*, \bar{\rho}^*+\rho'^*).&\end{aligned} \tag{5}$$

Substituting equation (5) into equations (1)–(4) and averaging over one tidal cycle, we obtain the equations governing mean currents

$$\begin{aligned}\overline{u'^*\frac{\partial u'^*}{\partial x^*}}+\overline{v'^*\frac{\partial u'^*}{\partial y^*}}+\overline{w'^*\frac{\partial u'^*}{\partial z^*}}+\bar{u}^*\frac{\partial \bar{u}^*}{\partial x^*}+\bar{v}^*\frac{\partial \bar{u}^*}{\partial y^*}+\bar{w}^*\frac{\partial \bar{u}^*}{\partial z^*}&\\ -f\bar{v}^*=-\frac{1}{\rho_0}\frac{\partial \bar{p}^*}{\partial x^*}+\upsilon\frac{\partial^2 \bar{u}^*}{\partial z^{*2}},&\end{aligned} \tag{6}$$

$$\begin{aligned}\overline{u'^*\frac{\partial v'^*}{\partial x^*}}+\overline{v'^*\frac{\partial v'^*}{\partial y^*}}+\overline{w'^*\frac{\partial v'^*}{\partial z^*}}+\bar{u}^*\frac{\partial \bar{v}^*}{\partial x^*}+\bar{v}^*\frac{\partial \bar{v}^*}{\partial y^*}+\bar{w}^*\frac{\partial \bar{v}^*}{\partial z^*}&\\ +f\bar{u}^*=-\frac{1}{\rho_0}\frac{\partial \bar{p}^*}{\partial y^*}+\upsilon\frac{\partial^2 \bar{v}^*}{\partial z^{*2}},&\end{aligned} \tag{7}$$

$$\frac{\partial \bar{u}^*}{\partial x^*}+\frac{\partial \bar{v}^*}{\partial x^*}+\frac{\partial \bar{w}^*}{\partial z^*}=0, \tag{8}$$

$$\frac{\partial \bar{p}^*}{\partial z^*}=-\bar{\rho}^* g. \tag{9}$$

Integrating equation (9) from a certain level z^* to the surface η^* and taking horizontal differences:

$$\Delta\bar{p}^*=\Delta\bar{\rho}^* g z^*+\rho_0 g\Delta\eta^*. \tag{10}$$

The equations are nondimensionalized by

$$[x^*]=L_X, [y^*]=L_Y, [z^*]=D, \left[\frac{\Delta\bar{\rho}^*}{\rho_0}\right]=\Phi, [\Delta\bar{\eta}^*]=\Pi$$

$$\begin{aligned}[u'^*]=U_T, [v'^*]=V_T, [\overline{u^*}]=U, [\overline{v^*}]=V, [\overline{w^*}]=\frac{D}{L_X}[\overline{u^*}]&\\ =\frac{DU}{L_X}.&\end{aligned}$$

The nondimensionalized equations (6) and (7) are written as

$$\begin{aligned}\frac{R_X\delta_U}{\delta_T^2}\left[\overline{u'\frac{\partial u'}{\partial x}}+\delta_L\overline{v'\frac{\partial u'}{\partial y}}+\overline{w'\frac{\partial u'}{\partial z}}\right]&\\ +R_x\delta_U\left[\left(\bar{u}\frac{\partial \bar{u}}{\partial x}++\bar{w}\frac{\partial \bar{u}}{\partial z}\right)+\frac{\delta_L}{\delta_U}\bar{v}\frac{\partial \bar{u}}{\partial y}\right)-\bar{v}=-P_\rho\frac{\partial \bar{\rho}}{\partial x}&\\ -P_\eta\frac{\partial \bar{\eta}}{\partial x}+E\delta_U\frac{\partial^2 \bar{u}}{\partial z^2},&\end{aligned} \tag{11}$$

$$\frac{R_X r}{\delta_T^2}\left[\overline{u'\frac{\partial v'}{\partial x}}+\delta_L\overline{v'\frac{\partial v'}{\partial y}}+\overline{w'\frac{\partial v'}{\partial z}}\right] + \frac{R_X}{\delta_U}\left[\left(\bar{u}\frac{\partial \bar{v}}{\partial x}+\bar{w}\frac{\partial \bar{v}}{\partial z}\right)+\frac{\delta_L}{\delta_U}\left(\bar{v}\frac{\partial \bar{v}}{\partial y}\right)\right]+\bar{u}=\frac{E}{\delta_U}\frac{\partial^2 \bar{v}}{\partial z^2}, \quad (12)$$

where

$$R_X=\frac{U}{fL_X},\ E=\frac{\nu}{fD^2},\ \delta_T=\frac{U}{U_T},\ \delta_U=\frac{U}{V},\ \delta_L=\frac{L_X}{L_Y},\ r=\frac{V_T}{U_T}$$
$$P_\rho=\frac{Dg\Phi}{fL_xV}, P_\eta=\frac{g\Pi}{fL_xV}, \quad (13)$$

and in equation (11) the pressure term is neglected assuming the along-frontal direction is almost aligned with the isobaths and that the tidal wave impinges onto the sloping bottom at a right angle.

[9] For the southern flank of Georges Bank, we choose typical scales for each variable:

$$L_X=10^4m, L_Y=10^5m, D=50m, U_T=10^0ms^{-1}, \Phi=10^{-3},$$
$$\Pi=10^{-2}m, U=10^{-2}ms^{-1}, V=2\times10^{-1}ms^{-1}, f=10^{-4}s^{-1},$$
$$\nu=10^{-2}m^2s^{-1}, r=0.5,$$

then

$$R_X=10^{-2}, E=4\times10^{-2}, \delta_T=10^{-2}, \delta_U=5\times10^{-2}, \delta_L=10^{-1},$$
$$P_\rho=2.5, P_\eta=0.5. \quad (14)$$

Substituting equation (14) into equation (11), it is shown that the mean along-shore current is balanced by the tidal stress term (the first term on the left side) and the pressure gradient, which agrees with *Loder* [1980]. It is noted that the cross-shore components in the tidal stress are one order larger than the along-shore component. Therefore to the lowest order, the equation (11) can be written as

$$\frac{R_X\delta_U}{\delta_T^2}\left[\overline{u'\frac{\partial u'}{\partial x}}+\overline{w'\frac{\partial u'}{\partial z}}\right]-\bar{v}=-P_\rho\frac{\partial\overline{\rho}}{\partial x}-P_\eta\frac{\partial\overline{\eta}}{\partial x}. \quad (15)$$

Similarly, substituting equation (14) into equation (12), in the lowest order, the cross-shore mean current is balanced by the tidal stress (cross-shore component) and the vertical mixing, thus equation (12) can be written as

$$\frac{R_X r}{\delta_T^2}\left[\overline{u'\frac{\partial v'}{\partial x}}+\overline{w'\frac{\partial v'}{\partial z}}\right]+\bar{u}=\frac{E}{\delta_U}\frac{\partial^2\bar{v}}{\partial z^2}. \quad (16)$$

Both equations (15) and (16) shows that the residual current associated with the tidal front on the southern flank of the Georges Bank has an approximately two-dimensional pattern (cross section). The analysis result is also confirmed by the comments by *Chen et al.* [2003] about the comparison between two-dimensional and three-dimensional model results. The two-dimensional flow pattern implies that when a passive tracer patch is moved from one place to another along the front by the along-frontal advection, the tracer could be considered a new release with different concentrations in terms of the cross-frontal movement.

3. Numerical Experiments

3.1. Model Configuration

[10] The Princeton ocean model (POM), a sigma-coordinate, free surface, and primitive-equation model [*Blumberg and Mellor*, 1987] is applied to the present study. In the model, the vertical mixing is parameterized using the *Mellor and Yamada* [1974] and *Mellor* [1982] level 2.5 turbulence closure scheme as modified by *Galperin et al.* [1988]. On the basis of the above scale analysis, the model used here is configured on a two-dimensional cross-bank plane (x-z) to focus on the cross-front process. The topography is in the form of an exponential function:

$$h=h_0\exp\left(\frac{x-x_0}{L}\right),\ \text{when } x_0<x, \quad (17)$$

$$h=h_0,\ \text{when } x<x_0,\ \text{and if } h>h_m, h=h_m,$$

where h_0 and h_m denote the water depths at the on-bank and off-bank sides, respectively, and L is the shelf width scale. Here we set h_0 = 30 m, h_m = 300 m, L = 10 km and x_0 = 20 km. The horizontal grid size is 500 m and the vertical grid consists of 40 equally spaced sigma levels. The time steps for the barotropic and baroclinic modes are 3s and 60s respectively. Semidiurnal tides (M_2) are imposed through a periodic surface displacement at the off-bank edge of the model domain, and a sponge layer appended to the onshore side attenuates the reflected waves. The amplitude of the surface elevation at the off-bank edge is chosen to be 0.5 m so that the tidal current at the on-bank side is about 1.0 m/s. Surface wind forcing and heat fluxes are not considered. The radiation condition and sponge layer (40 grid points) are set at both inshore and offshore boundaries.

[11] The multidimensional positive definite advection transport algorithm (MPDATA) [*Smolarkiewicz*, 1984; *Smolarkiewicz and Clark*, 1986; *Smolarkiewicz and Grabowski*, 1990] is utilized in the advection scheme. No additional horizontal diffusivity is needed for this resolution. MPDATA is usually configured as a sign-preserving scheme, which is particularly important in problems where erroneous, negative concentrations would otherwise arise if the standard second-order centered scheme is used instead. The basic concept of the scheme is the successive application of an upwind scheme with correction to the first-order truncation error using antidiffusion velocity. The repeated procedure yields a positive definite advection algorithm with second-order accuracy. The flux correction of MPDATA protects against over- and under-shoot where the gradients are more extreme [*Hecht et al.*, 2000]. For the further comparison of several advection schemes, please refer to *Pietrzak* [1998].

[12] The temperature is used as a proxy for the density field (salinity is kept constant at 32.8 psu). The initial temperature field increases linearly from 6.0°C to 10.0°C between the depth 33m and 42m, corresponding to a density range between 25.4 and 25.8 in σ_t unit, which is representative of the southern flank of Georges Bank

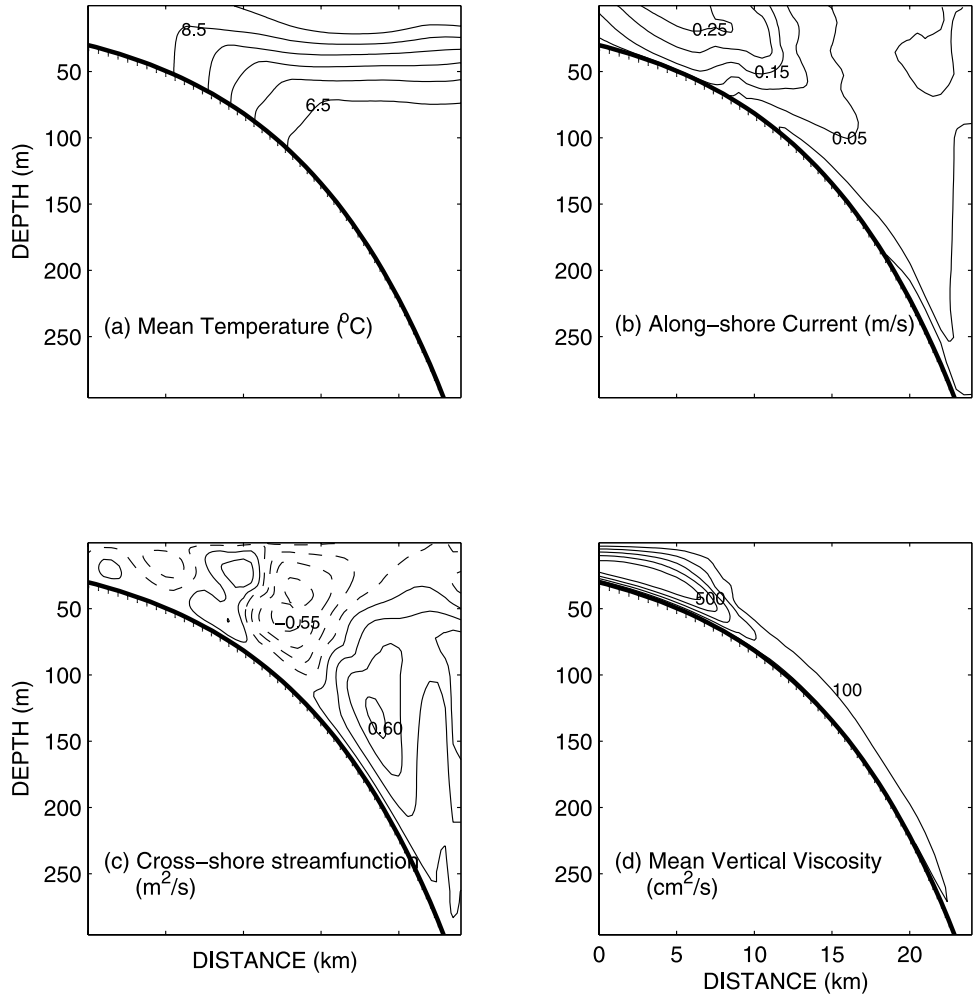

Figure 1. (a) The mean temperature distribution (°C). The contour interval is 0.5°C. (b) The alongshore mean current (m/s). The contour interval is 0.05 m/s. (c) The cross-shore Eulerian stream function (m^2/s). The contour interval is 0.11 m^2/s. (d) The mean vertical viscosity (cm^2/s), and the contour interval is 100 cm^2/s.

[*Houghton and Ho*, 2001]. After integrating for 10 tidal cycles starting from a state of rest, a quasi-equilibrium state is reached and a tidal front is formed with two branches, one of which outcrops to the surface and another intersects the bottom, shown in Figure 1a. The Eulerian along-frontal current (Figure 1b) flows in the direction with the shallow water on the right side. The Eulerian cross-frontal circulation (Figure 1c) is in a multiple-cell structure [*Dong et al.*, 2004; Dong et al., submitted manuscript, 2003]. The vertical viscosity decreases dramatically in the frontal zone due to the presence of stratification. These model results are in general agreement with the hydrographic observations [*Loder and Brickman*, 1992] and previous three-dimensional model experiments on the Georges Bank conducted by *Naimie et al.* [1994] and *Naimie* [1996] using the Dartmouth finite element model and *Chen et al.* [2001, 2003] using the Ecom-si finite difference model.

[13] At the 11th tidal cycle, a passive tracer patch is released into the water. The patch initially occupies one grid point horizontally and two grid points vertically (one grid point away from the bottom), and its concentration is set to unity. After the tracer is released, the model runs for 5 more tidal cycles. During this period, the tracer inventory is calculated and it stays nearly constant with a slight oscillation (the amplitude of the oscillation is only 0.1% of the initial inventory). A series of numerical experiments are performed with tracer releases at different tidal phases and locations within the front. The details of the experiments are summarized in Table 1. The first experiment (experiment 1) is the basic one. Experiments 1, 2, 3, and 4 have the same release tidal phase but different release locations, while experiments 1, 5, 6, and 7 are at the same release location but at different release tidal phases.

3.2. Quantifying the Movement of the Tracer Patch

[14] Before presenting the numerical results of the passive tracer, we first discuss how to calculate the movement of the tracer relative to the isopycnals (isotherms) that define the front. In this paper, we use a method suggested by *Houghton and Ho* [2001] and *Houghton* [2002] to estimate the dye patch movement. In the following, we generalize the method.

Table 1. Summary of Experiments[a]

Experiment	Release Position	Tidal Phase
1	offshore edge of the front (6.5°C)	slack before ebb
2	inside the front (7.0°C)	slack before ebb
3	inside the front (7.5°C)	slack before ebb
4	inshore edge of the front (8.0°C)	slack before ebb
5	offshore edge of the front (6.5°C)	peak ebb
6	offshore edge of the front (6.5°C)	slack before flood
7	offshore edge of the front (6.5°C)	peak flood

[a]Note that peak ebb denotes the moment when the seaward tidal current reaches its maximum; peak flood denotes the moment when the shoreward tidal current reaches its maximum; slack before ebb denotes the moment when the tidal current starts to flow seaward; slack before flood denotes the moment when the tidal current starts to flow shoreward. All the phases is that of the tidal current at the offshore edge.

[15] The temperature of a tracer patch is defined as a dye concentration-weighted mean temperature:

$$T(t) = \left(\int_S C(x,z,t)\theta(x,z,t)dxdz \right) / C_0, \tag{18}$$

where C(x, z, t) and θ (x, z, t) are the tracer concentration and isotherm at the point (x, z) at the time t, respectively, C_0 is the total tracer inventory (constant), S is the whole domain and T(t) denotes the patch temperature at time t. In the mixing layer where a tracer spreads, the horizontal position, where the temperature θ (x, z, t) is equal to the patch temperature T(t), is defined as the tracer patch center X(t). It is noted that the vertical position could be any level (here two grids from bottom chosen) since the isotherms are vertical in the mixing layer.

[16] The isothermal position $\chi(\theta, t)$ is defined as the position (two grid points above the bottom) where θ is the temperature at the position at time t. Using the two positions X(t) and $\chi(\theta, t)$, the diapycnal velocity of the tracer patch is

$$V(\theta,t) = \frac{[X(t+\Delta t) - \chi(\theta, t+\Delta t)] - [X(t) - \chi(\theta,t)]}{\Delta t}, \tag{19}$$

or

$$V(\theta,t) = \frac{X(t+\Delta t) - X(t)}{\Delta t} - \frac{\chi(\theta,t+\Delta t) - \chi(\theta,t)}{\Delta t}. \tag{20}$$

In equation (20), the first term on the right side is the movement of the tracer patch relative to the isotherm and the second term is the movement of the isotherm. Equation (20) tells us the diapycnal velocity is the velocity of the patch relative to a certain isotherm minus the isotherm velocity. However, the isotherm used varies with time and the movements of different isotherms are different, therefore relative to different isotherms, the diapycnal velocity defined in equation (20) may vary, namely it is a function of θ. This can be seen in the following experiment results.

[17] There is a special situation, when isothermal diffusion can be neglected and the second term in equation (20) is independent of θ so that the diapycnal velocity does not rely on any particular isotherm. This was the assumption used in the analysis of the field data by *Houghton and Ho* [2001]. Now the velocity over one tidal cycle is simplified as

$$V(t) = \frac{X(t+\tau) - X(t)}{\tau}, \tag{21}$$

where τ is the tidal period and the second term in equation (20) is zero because the isotherm returns to its starting point after one tidal cycle.

[18] In general, let D(θ, t) denote the relative distance between the tracer center and the isotherm θ

$$D(\theta,t) \equiv X(t) - \chi(\theta,t), \tag{22}$$

then for Δt infinitely small, and equations (19) or (20) becomes

$$V(\theta,t) = \frac{dD(\theta,t)}{dt}. \tag{23}$$

3.3. Basic Experiment

[19] In experiment 1, a tracer patch is released near the bottom of the off-bank side of the front at the slack before ebb, where the thickness of the bottom mixing reaches its maximum and the isotherms below the thermocline level are almost vertical (see Figures 2a and 2b). During the previous flood, when the tidal flow is on-bank, the shear near the bottom carries colder water over warmer water, resulting in a strong convection that intensifies vertical mixing. The evolution of the tracer concentration in the 1st and 5th tidal cycles is plotted in Figures 2a and 2b, respectively. Five snap shots are presented in each cycle: the slack before ebb (initial state), the peak ebb, the slack before flood, the peak flood, and the next slack before ebb. The tracer concentration is normalized by its maximum in each section. In Figure 2a, it can be seen that the tracer patch in the 1st tidal cycle moves back and forth with the tide and is vertically mixed and horizontally diffused. At the end of the tidal cycle (the next slack before ebb) the tracer moves on-bank relative to the isotherms. Figure 2b shows the tracer in the 5th tidal cycle, when the tracer patch has spread through the frontal area underneath the stratification. The tracer as a whole appears to be displaced onshore relative to the frontal isotherms.

[20] On the basis of equation (18), the concentration-weighted mean tracer patch temperature is calculated at every time step and plotted in Figure 3 (solid line). The patch temperature increases with time. Initially it is about 6.5°C, and at the end of the fifth tidal cycle it increases to more than 7.0°C. The stratification prevents the tracer from penetrating the thermocline, therefore the increase in patch temperature is mainly caused by the on-bank movement.

[21] In order to obtain a quantitative estimate of the tracer movement, based on the method introduced in section 3b, the values of the patch temperature are marked onto the temperature field in the bottom mixed layer to locate the patch center position X(t), which is plotted in Figure 4 (the thickest line). The oscillation represents the tracer movement back and forth with the tide. The positions of isotherms 6.5°C, 7.0°C, 7.5°C and 8.0°C are also plotted in Figure 4 (light lines). This illustrates clearly how the tracer patch crosses the isotherms that define the tidal front, as the

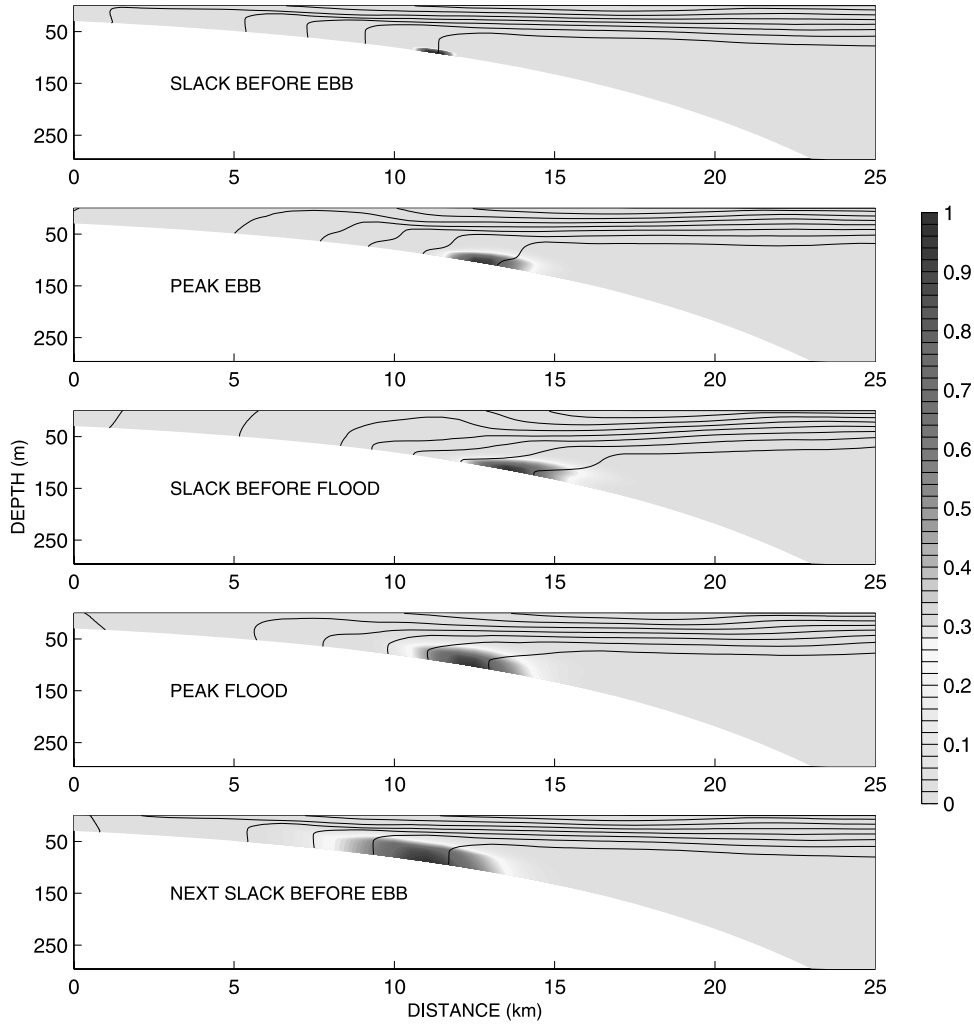

Figure 2a. Four snap shots of the concentration distribution of passive tracer (normalized by its maximum in each section) for experiment 1 in the 1st tidal cycle. The contour lines (black) are the isotherms (contour interval is 0.5°C from 6.5°C to 9.0°C). The text in the figure denotes the tidal phase when the tracer distribution is presented.

tracer patch moves on-bank toward the warmer side of the front. The horizontal diffusion of temperature is seen as the gradual divergence of the isotherms.

[22] The velocity relative to each isotherm is calculated and the speeds are plotted in Figure 5 for successive tidal cycles. The speeds differ for different isotherms as expected, but the trend, decreasing with time, is the same. The average speed relative to all isotherms (sampled every 0.1°C from 6.5°C to 8.0°C), which may be considered the velocity of the tracer patch relative to the whole front, is calculated and plotted in Figure 5 (solid line). The velocity, directed on-bank, is 2.4 cm/s in the 1st cycle, and drops to 0.5 cm/s in the 5th cycle.

3.4. Sensitivity to the Release Position

[23] In order to assess the effect of the release position within the tidal front on the tracer dispersion, three experiments (experiments 2, 3, and 4) were performed. Using the same method as that in section 3c, the patch temperature and averaged velocity in each tidal cycle for each experiment are calculated and plotted in Figures 3 and 6, respectively (for comparison, the velocity for experiment 1 is also plotted in Figure 6). For all experiments except experiment 4, the tracer moves monotonically from the cold water to warm water, and the diapycnal speed decreases with time. For experiment 2, the tracer is initially released at about 7.0°C; it moves to 7.5°C in five tidal cycles (dashed line in Figure 3). Its velocity is 2.1 cm/s in the 1st tidal cycle, and drops to 0.3 cm/s in the 5th tidal cycle (dashed line marked with circles in Figure 6). For experiment 3, the tracer is released at 7.5°C and moves to 7.8°C in 5th cycles (dotted-dashed line in Figure 3). Its velocity is 2.4 cm/s in the 1st cycle and drops to 0.2 cm/s in the 5th tidal cycle (dashed-dotted line marked with squares in Figure 6). The comparison among the three experiments shows that the farther on-bank a tracer is released the smaller the decrease in temperature.

[24] For experiment 4, in when the tracer is released at the inshore edge of the front, one may note from Figure 3 that, compared with experiments 1, 2, and 3, the trend of the tracer temperature is different. In the 1st cycle, the temper-

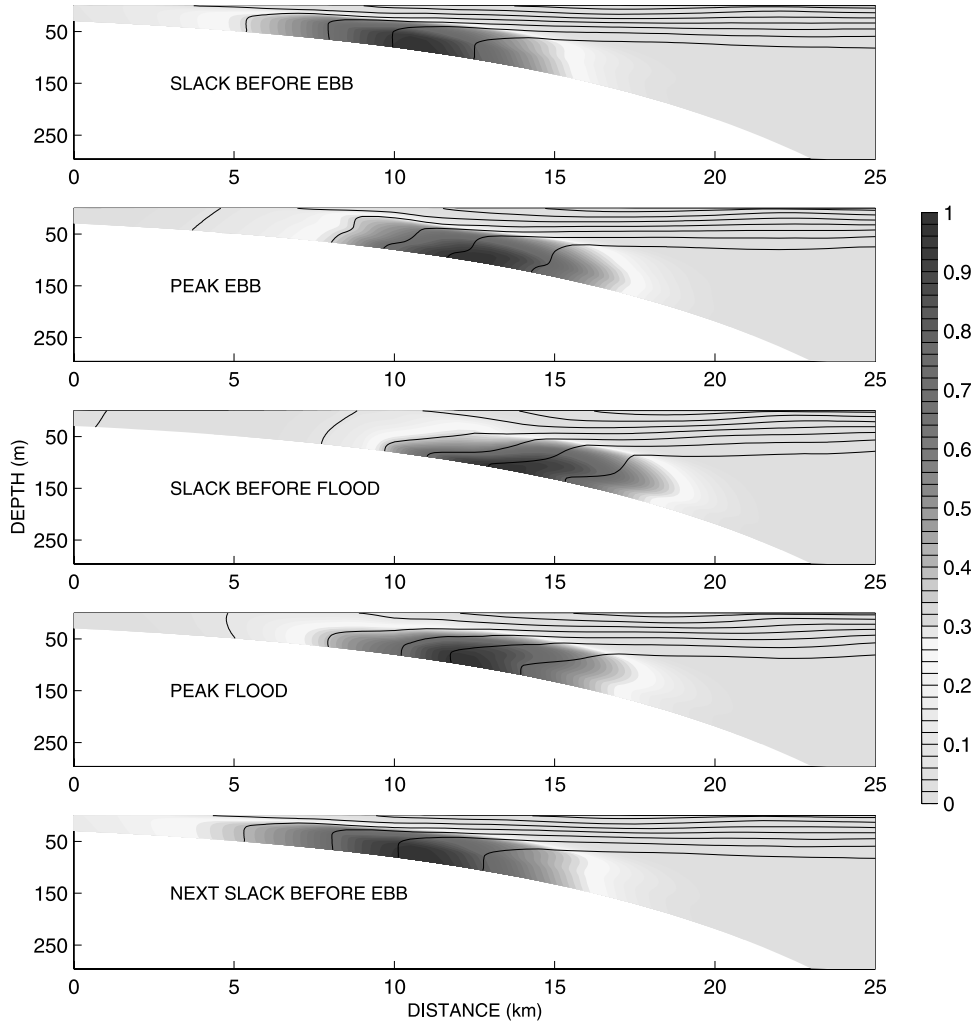

Figure 2b. The same as Figures 2a except for the 5th tidal cycle.

ature increases slightly, and then starts to decrease. Figures 7a and 7b show the snap shots of the tracer distribution in the 1st and 5th tidal cycles, respectively. In the 1st cycle, part of the tracer has moved offshore along the isotherm into the lower layer of the stratification, and by the 5th cycle the tracer is partially mixed back to the middepth, which causes the temperature of tracer to decrease. While the tracer moves into the stratified layer, the assumption that a tracer stays in the bottom mixed layer for the above method to calculate the diapycnal velocity is not satisfied. Therefore the velocity for experiment 4 is not shown in Figure 6. In summary, these four experiments show that the tracer dispersion is dependent on the release position, with the biggest differences between the tracers released at the offshore and inshore sides of the front.

3.5. Sensitivity to the Release Tidal Phase

[25] Does the tidal phase during release affect the tracer dispersion? This is a practical question concerned by people conducting field experiments with tracers. With the same configuration as in experiment 1 except for the release tidal phase (experiment 1 was at the slack before ebb), experiments 5, 6, and 7 were conducted with the tracer released at peak ebb, peak flood, and slack before flood, respectively, to examine the effect of tidal phase. The time dependence of the tracer patch temperature for experiments 1, 5, 6, and 7 is shown in Figure 8. The comparison shows a similar trend with slight differences. It demonstrates that the tidal phase at the time of release does not affect the tracer dispersion significantly.

4. Comparison With the Dye Experiment

[26] With an idealized model as the above two-dimensional one, a precise simulation of the dye tracer experiment by *Houghton and Ho* [2001] is not intended in this study. As the first step to understand the physical processes involved, the qualitative comparison of the above numerical results with the field experiment is still intriguing.

[27] In the field experiment, the tracer was injected in the bottom mixed layer on the seaward side of the tidal front. Figure 9 shows the tracer distributions at two times after injection into the bottom of the front on the southern flank. The significant movement from the cold water to warm water (on-bank) is observed. More

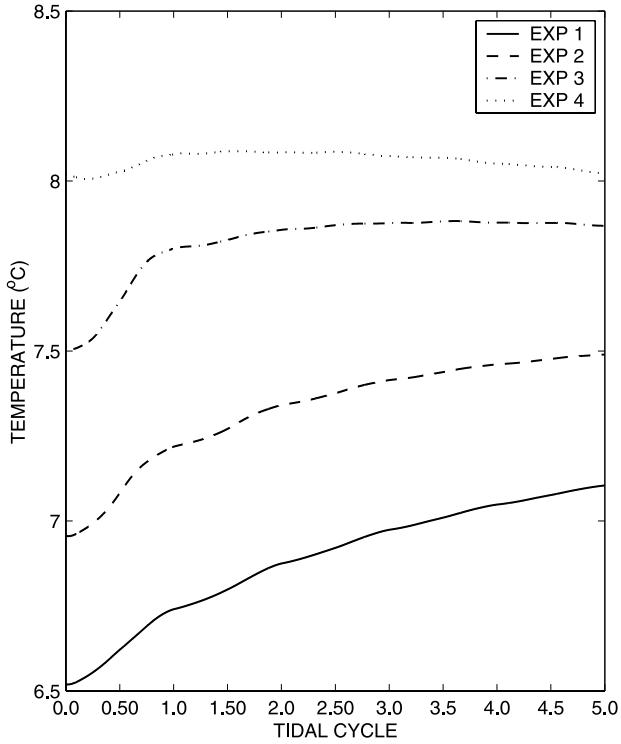

Figure 3. The concentration-weighed mean patch temperature variation with time. The solid line is for experiment 1, dashed line is for experiment 2, dashed-dotted line is for experiment 3, and dotted line is for experiment 4.

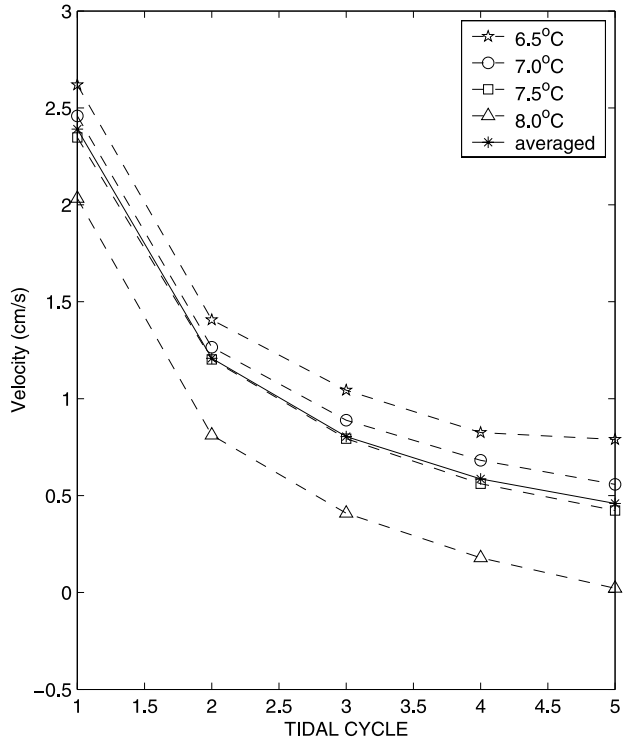

Figure 5. The velocity of the tracer relative to individual isotherms (dashed lines) in each tidal cycle and the averaged velocity relative to all isothermals (every 0.1°C from 6.5°C to 8.0°C) (solid line) for experiment 1.

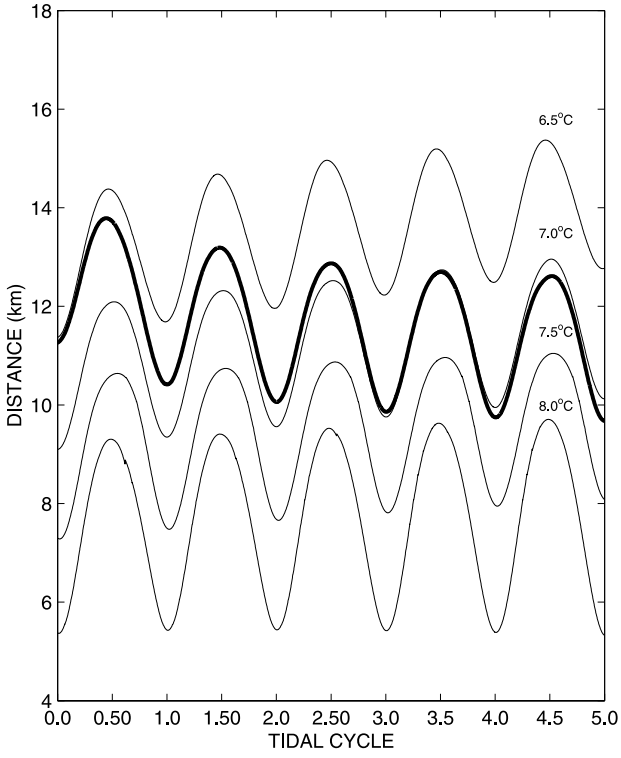

Figure 4. The tracer centroid and isotherm across-bank movement with time for experiment 1. The thickest line denotes the tracer and light line the isotherms. The text denotes the temperature of the isotherm.

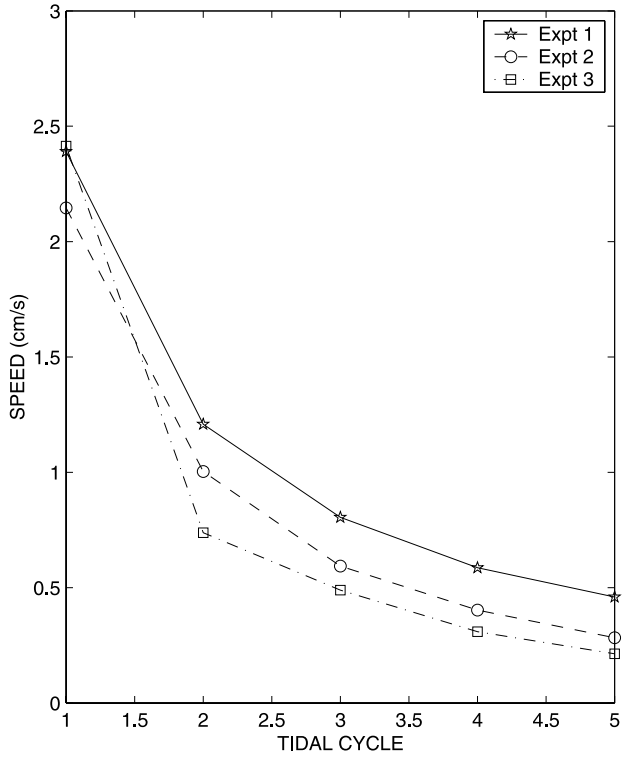

Figure 6. The averaged tracer velocity at the end of the each tidal cycle. The solid line is for experiment 1, dashed line is for experiment 2, and dashed-dotted line is for experiment 3.

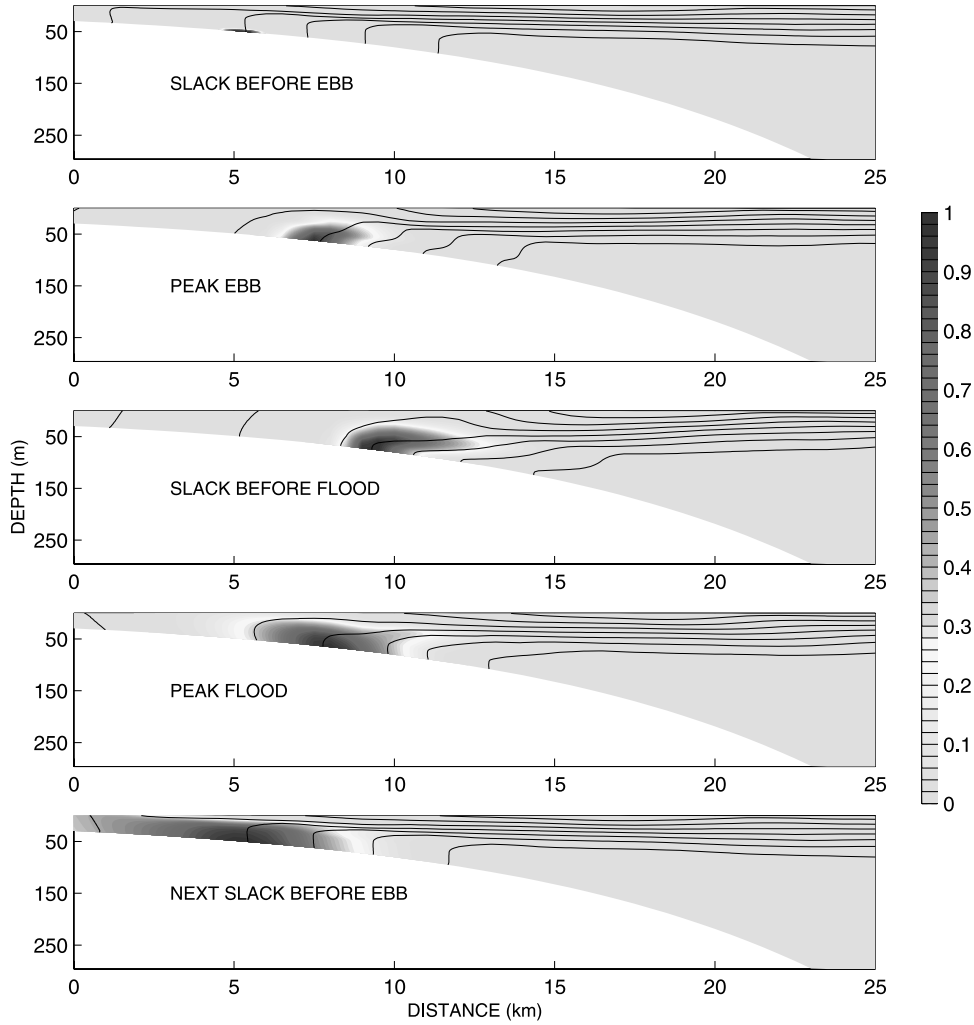

Figure 7a. The same as Figure 2a except for experiment 4.

details about the field experiment can be found in the work of *Houghton and Ho* [2001] and *Houghton* [2002]. The primary results in the field experiment are the tracer patch moves on-bank after it is released at the foot of the offshore tidal front and its speed decreases with time. The dye patch moved on-bank through the tidal front in approximately three days. The dye patch velocity was calculated from

$$V = \frac{dT_p/dt}{dT/dx}, \tag{24}$$

where T_p is the concentration weighted patch average temperature and dT/dx is the cross-bank temperature gradient in the bottom mixed layer evaluated at $T = T_p$.

[28] To calculate T_p, the patch integration was extended from the bottom up to 18 m depth to exclude the warming due to vertical mixing of the dye into the thermocline above that depth. The resulting on-bank velocities as a function of the distance across the tidal front (Figure 10) are qualitatively consistent with model calculations from experiment 1 using the average curve in Figure 5. Both the field and numerical experiments show the on-bank tracer movement with speeds decreasing with the distance from the original release point. Speeds are in the same order: 1 cm/s. The qualitative agreement between the model and field experiments further shows the two-dimensional model can catch the essential dynamics in the problem. Owing to the limitation of the two-dimensional model, the advection along the front can not be simulated in the present study, which limits the complete comparison of model results with the field data, such as the concentration variation with time.

5. Comparison With Lagrangian Velocity

[29] Both field and numerical experiments show that the passive tracer patch moves on-bank through the tidal front with speed decreasing with time. A passive tracer reflects the movement of its tagged water, i.e., the Lagrangian flow. However, the Lagrangian velocity is generally defined by a single fluid particle trajectory. The tracer velocity is an average over a patch that is mixed into an increasingly volume. Therefore the velocity inferred from the tracer patch maybe differs from a local Lagrangian velocity. However, the structure of the model derived Lagrangian velocity could be used to interpret the model and observational tracer patch results.

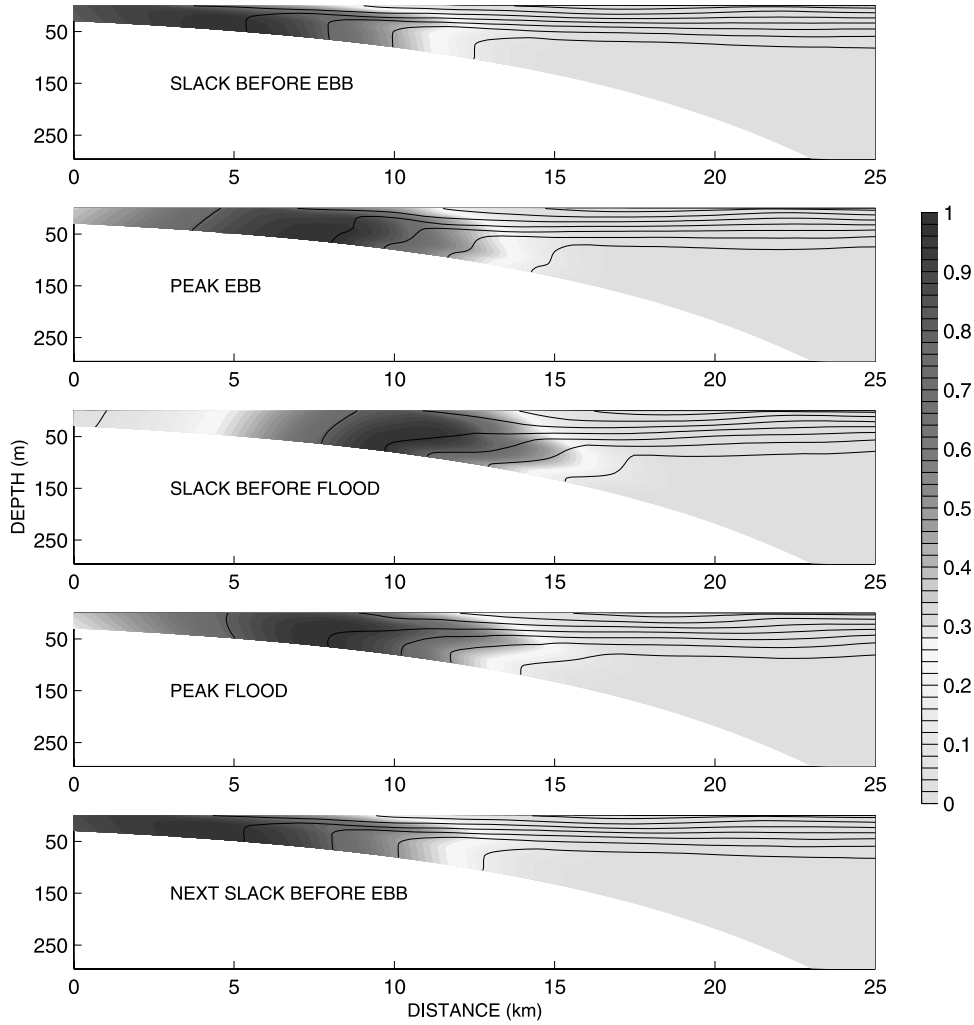

Figure 7b. The same as Figure 2b except for experiment 4.

[30] The model Lagrangian velocity field is calculated at each grid point from the trajectory of the fluid parcel over a tidal cycle starting at the slack before ebb of the 11th tidal cycle. Figure 11a shows the trajectories of fluid parcels over 5 tidal cycles. In the bottom layer, the parcels move on-bank. At the inshore side of the front, parcels in the upper layer move off-bank forming a clockwise cell. The Lagrangian velocity field (Figure 11b) is derived from the net displacement of the water parcel in one tidal cycle assigned to the position of the initial grid point. In the bottom mixed layer the on-bank flow decreases on both sides of the tidal front. Away from the bottom, the on-bank flow decreases. On the on-bank side of the front, the circulation has two distinct layers: off-bank in the upper layer and on-bank in the bottom layer. The off-bank flow becomes a middepth tongue in the stratified layer that deepens as it moves across the tidal front. The Lagrangian velocity structure reflects the cross-front variation in the Eulerian velocity and Stokes drift [*Longuet-Higgins*, 1969].

[31] The Lagrangian circulation described above is in general consistent with previous model experiments by *Loder et al.* [1997] and *Chen and Beardsley* [1998] and *Chen et al.* [2003]. That the on-bank bottom flow is larger than that by *Loder et al.* [1997] is because of the presence of the tidal front.

[32] This Lagrangian velocity distribution may be used to interpret the patch velocity. When a tracer is released near the bottom, it moves on-bank following the fluid particle as shown in the Lagrangian flow. As the tracer is mixed vertically to where the Lagrangian velocity decreases and even changes its direction, the patch velocity, a concentration-weighted mean, decreases reflecting the Lagrangian flow structure. Thus the decrease in the on-bank velocity shown in Figure 10 is more abrupt than the decrease of the near bottom Lagrangian field shown in Figure 11b.

[33] We recalculate the tracer patch velocity using a concentration-weighted average as before but now using the Lagrangian velocity field directly rather than using the tracer displacement relative to the thermal field as done in the initial calculation (Figures 5 and 6). The results for experiments 1–3 are shown in Figure 12. The velocities decrease with time even though the on-bank velocity at the bottom continues to increase onshore within the tidal front (Figure 11b). This is because of the vertical mixing of the tracer up into the water column where the on-bank flow is weaker. In experiment 4 (not shown) where the tracer is released on the on-bank side

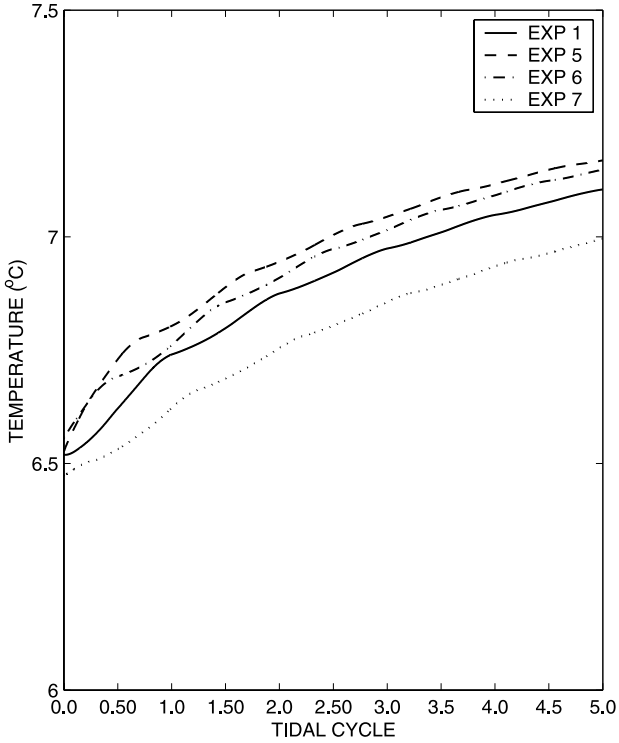

Figure 8. The concentration-weighted mean patch temperature variation with time. The solid line is for experiment 1, dashed line is for experiment 5, dashed-dotted line is for experiment 6, and dotted line is for experiment 7.

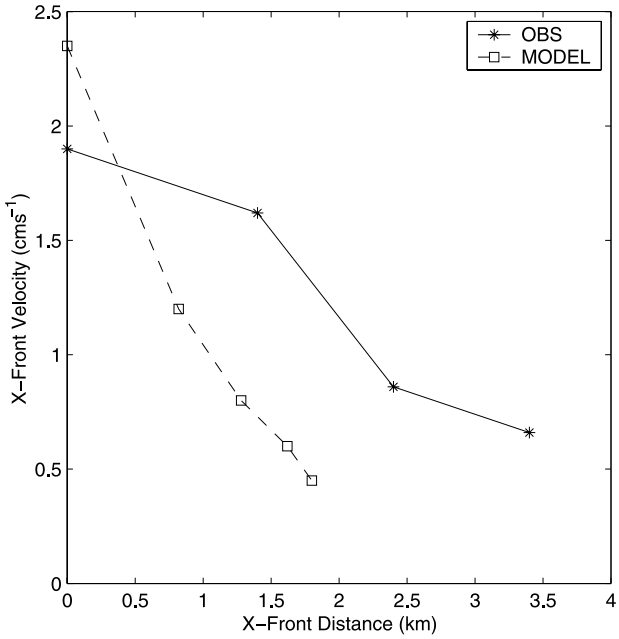

Figure 10. The on-bank velocity as a function of cross-front distance for the south flank Georges Bank dye experiment (solid line) and model calculation experiment 1 (dashed line).

of the front, the tracer rapidly mixes into the base of the stratified layer where the flow is off-bank (Figure 11b). The Lagrangian circulation moves the tracer down and off-bank into cooler water explaining the slow cooling shown in Figure 3 (dotted line) following the first tidal cycle.

6. Discussion

[34] The two-dimensional model results presented here are in general consistent with previous three-dimensional model experiments on Georges Bank in Eulerian and Lagrangian flows [*Naimie et al.*, 1994; *Naimie*, 1996; *Loder et al.*, 1997; *Chen et al.*, 2001, 2003]. However, in a two-dimensional model, the absence of the along-frontal dispersion of the tracer may lessen the spread of the tracer patch. In a theoretical study on the decay of a passive tracer, *Sukhatme and Pierrehumbert* [2002] indicated the size of a passive tracer patch may affect the net transport of the tracer. A two-dimensional circulation pattern is only an approximation to the reality in the lowest order in the southern flank of Georges Bank. To implement a realistic simulation of the dye trace experiment, a three-dimensional model must be employed with the real hydrography and topography.

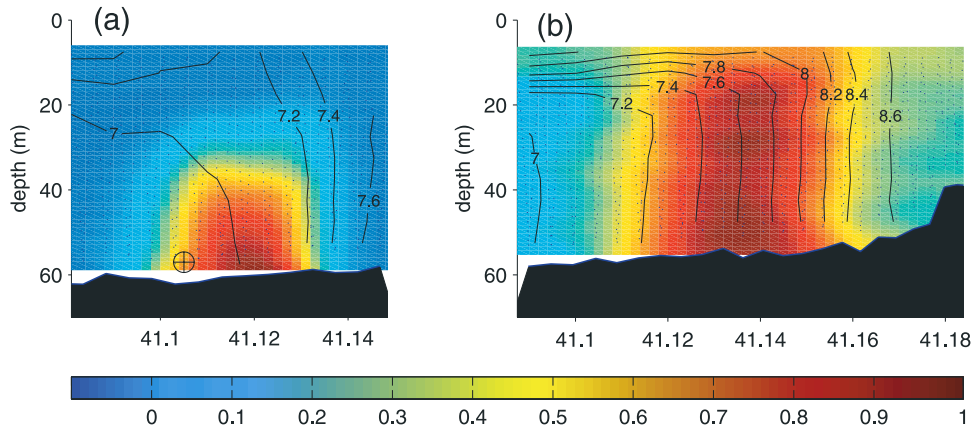

Figure 9. Cross-frontal sections of dye concentration, normalized by the maximum in the section (a) 16 hours and (b) 85 hours after injection. The relative location of the dye injection site is given by the plus circle and the Scanfish track by the dotted line. Temperature contour interval is 0.1°C.

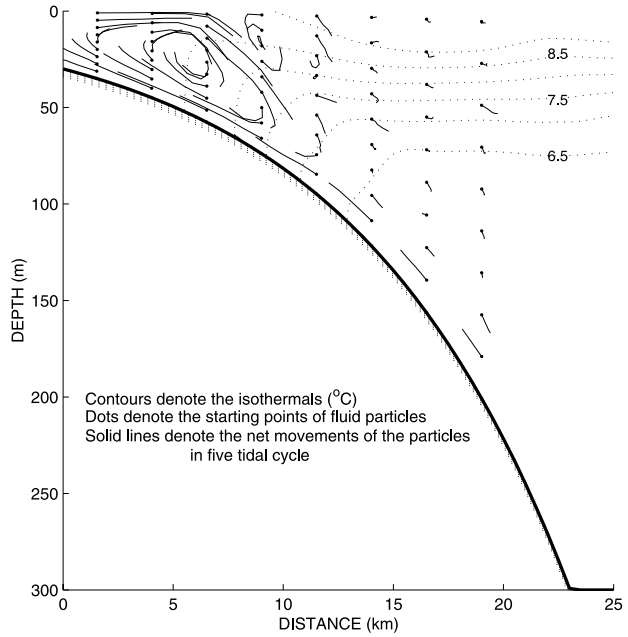

Figure 11a. The fluid parcel trajectories over five tidal cycles.

[35] There is an assumption behind the method of calculating the diapycnal velocity of a tracer patch (section 3b) and the dye analysis [*Houghton and Ho*, 2001]: that the change in the tracer temperature is mainly caused by its horizontal movement. In their analysis of the time dependence of the dye patch temperature the temperature calculation was cut-off at 18 m depth to minimize patch warming due to mixing into the near surface thermocline. The close agreement of the two model tracer calculations by patch temperature changes (Figure 6) and the Lagrangian velocity field (Figure 12) indicates that vertical mixing into the thermocline has a minimal effect. Instead the cross-front variation of the on-bank tracer velocity (Figure 10) is due primarily to the vertical structure of the Lagrangian velocity and its contribution to the patch velocity as the tracer mixes vertically and the concentration-weighted integration extends further up through the water column. The on-bank decrease of the on-bank flow in the bottom of the tidal front (Figure 11b) is much more gradual than the decrease of the patch velocity (Figure 10).

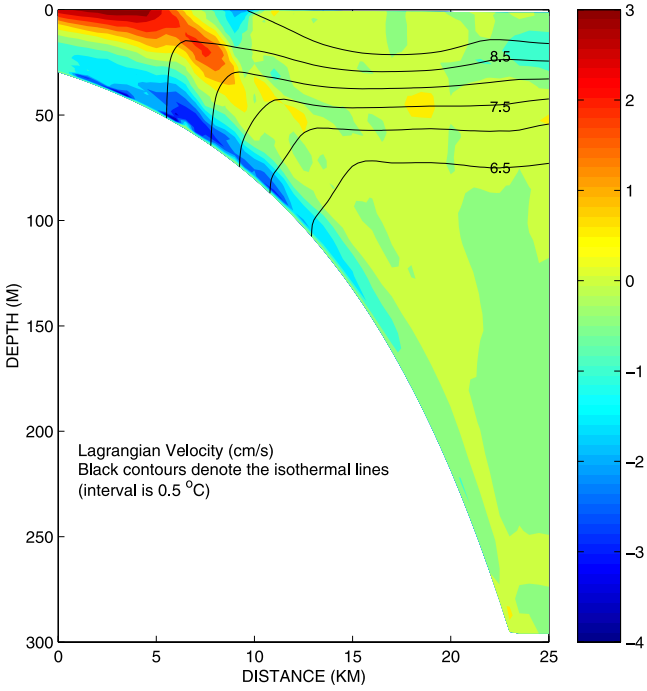

Figure 11b. The horizontal Lagrangian velocity distribution in one tidal cycle. Isotherms are contoured with an interval of 0.5°C.

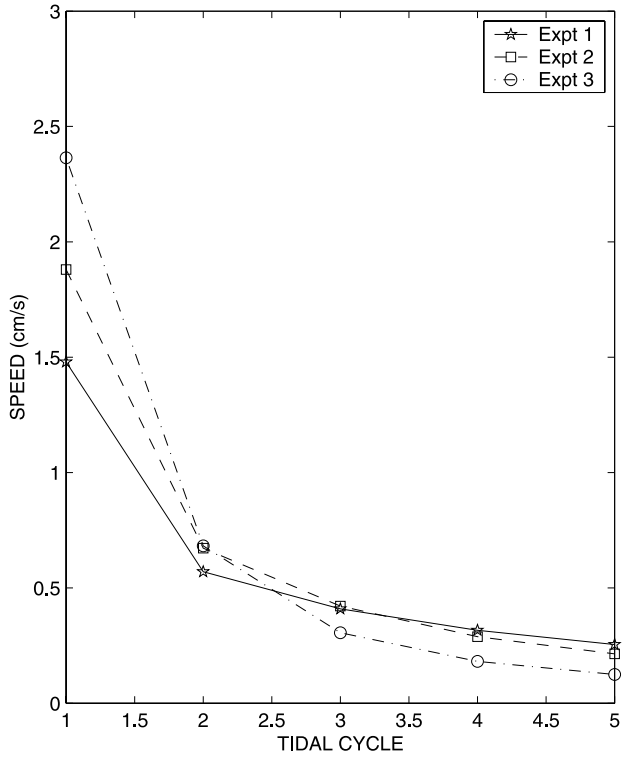

Figure 12. The concentration-weighted mean Lagrangian velocity for experiments 1, 2, and 3 in each tidal cycle. The solid line is for experiment 1, dashed line is for experiment 2, and dashed-dotted line is for experiment 3.

[36] Although the tidal model is quasi-steady state, diffusive spreading of the isotherms defining the front is evident in Figure 4. This generates a range of patch velocities when defined to different isotherms (Figure 5). This effect is not negligible but is sufficiently small to not affect the basic model results or to negate the assumption used in the dye tracer analysis.

7. Conclusions

[37] Using a two-dimensional version of Princeton oceanic model, a series of numerical experiments with passive tracers are performed to study the diapycnal flow through a tidal front. In the basic experiment, a tracer is released at the offshore edge of a tidal front, and the results qualitatively agree well with a field experiment on the Georges Bank: the

tracer moves on-bank with a diapycnal velocity that decreases with time.

[38] Additional experiments were performed to investigate the sensitivity of the tracer dispersion to the tidal phase and location of the tracer release within the front. As the release point is moved on-bank across the front, the tracer velocity decreases until at the on-bank edge of the front it reverses weakly. This trend can be understood by considering the structure of the Lagrangian velocity field in the tidal front and the degree of vertical mixing of the tracer.

[39] Tracer motion is calculated by two methods, directly from the model Lagrangian velocity field and indirectly from changes in the tracer patch average temperature and hence its position in the front. The close agreement of these two methods shows that the tracer movement represents the weighted-averaged Lagrangian velocity over the area the tracer spreads other than at a single point. It also justifies the assumption that the change in the tracer temperature is primarily contributed by its cross-front movement and that frontal expansion by diffusion is minimal. The on-bank decrease in the on-bank velocity is primarily due to the increasing contribution of the flow field throughout the water column as the tracer mixes vertically in the course of its traverse through the front.

[40] **Acknowledgments.** We wish to acknowledge Martin Visbeck, Arnold Gordon, and Robin Robertson from Columbia University, Robert Wilson from State University of New York at Stony Brook, and George Mellor from Princeton University for their valuable comments and suggestions. Support for the study is provided by NSF grants NSF/ATM 96-18260, RH by OCE-9806361 and 0236270 and TE by ONR grant N000140010228. Two anonymous reviewers provided excellent comments and suggestions that improved the paper. This is Lamont-Doherty Earth Observatory contribution 6591.

References

Blumberg, A. F., and G. L. Mellor (1987), A description of a three-dimensional coastal ocean circulation model, in *Three-Dimensional Coastal Models*, *Coastal Estuarine Sci.*, vol. 4, edited by N. Heaps, pp. 1–16, AGU, Washington, D. C.

Butman, B., and R. C. Beardsley (1987), Long-term observations on the southern flank of Georges Bank: Part I. A description of the seasonal cycle of currents, temperature, stratification, and wind stress, *J. Phys. Oceanogr.*, *17*, 367–384.

Chen, C., and R. C. Beardsley (1998), Tidal mixing and cross-front particle exchange over a finite amplitude asymmetric bank: A model study with application to Georges Bank, *J. Mar. Res.*, *56*, 1163–1201.

Chen, C., R. Beardsley, and P. J. S. Franks (2001), A 3-D prognostic numerical model study of the Georges Bank ecosystem, part I. Physical model, *Deep Sea Res. Part II*, *48*, 419–456.

Chen, C., Q. Xu, R. C. Beardsley, and P. J. S. Franks (2003), Model study of the cross-frontal water exchange on Georges Bank: A three-dimensional Lagrangian experiment, *J. Geophys. Res.*, *108*(C5), 3142, doi:10.1029/2000JC000390.

Dong, C., H.-W. Ou, D. Chen, and M. Visbeck (2004), Tidally induced cross-front mean circulation: Analytical study, *J. Phys. Oceanogr.*, *34*, 293–305.

Galperin, B., L. H. Kantha, S. Hassid, and A. Rosati (1988), A quasi-equilibrium turbulent energy model for geophysical flows, *J. Atmos. Sci.*, *45*, 55–62.

Garrett, C. J. R., and J. W. Loder (1981), Dynamical aspects of shallow sea fronts, *Philos. Trans. R. Soc. London A*, *302*, 563–581.

Hecht, M. W., B. Wingate, and P. Kassis (2000), A better, more discriminating test problem for ocean tracer transport, *Ocean Model.*, *2*, 1–15.

Houghton, R. (2002), Diapycnal flow through a tidal front: A dye tracer study on Georges Bank, *J. Mar. Syst.*, *37*, 31–46.

Houghton, R., and C. Ho (2001), Diapycnal flow through the Georges Bank tidal front: A dye tracer study, *Geophys. Res. Lett.*, *28*, 33–36.

Limeburner, R., and R. C. Beardsley (1996), Near surface recirculation of Georges Bank, *Deep Sea Res. Part II*, *43*, 1547–1574.

Loder, J. W. (1980), Topographic rectification of tidal currents on the sides of Georges Bank, *J. Phys. Oceanogr.*, *10*, 1399–1416.

Loder, J. W., and D. Brickman (1992), Detailed structure of currents and hydrography on the northern side of Georges Bank, *J. Geophys. Res.*, *97*, 14,331–14,351.

Loder, J. W., and D. G. Wright (1985), Tidal rectification and frontal circulation on the sides of Georges bank, *J. Mar. Res.*, *43*, 504–581.

Loder, J. W., K. F. Drinkwater, N. S. Oakey, and E. P. Horne (1993), Circulation, hydrographic structure and mixing at tidal fronts: The view from Georges Bank, *Philos. Trans. R. Soc. London A*, *343*, 447–460.

Loder, J. W., W. Y. Shen, and H. Ridderinkhof (1997), Characterization of three- dimensional Lagrangian circulation associated with tidal rectification over a submarine bank, *J. Phys. Oceanogr.*, *27*, 1729–1742.

Longuet-Higgins, M. S. (1969), On the transport of mass by time-varying ocean currents, *Deep Sea Res.*, *16*, 431–447.

Lynch, D. R., J. T. C. Ip, C. E. Naimie, and F. E. Werner (1996), Comprehensive coastal circulation model with application to the Gulf of Maine, *Cont. Shelf Res.*, *16*, 875–906.

Mellor, G. L. (1982), Development of a turbulence closure model for geophysical fluid problem, *Rev. Geophys. Space Phys.*, *20*, 851–875.

Mellor, G. L., and T. Yamada (1974), A hierarchy of turbulence closure models for planetary boundary layers, *J. Atmos. Sci.*, *33*, 1791–1796.

Naimie, C. E. (1996), Georges Bank residual circulation during weak and strong stratification periods: Prognostic numerical model results, *J. Geophys. Res.*, *101*(C3), 6469–6489.

Naimie, C. E., J. W. Loder, and D. R. Lynch (1994), Seasonal variation of the three- dimensional residual circulation on Georges Bank, *J. Geophys. Res.*, *99*, 15,967–15,989.

Naimie, C. E., R. Limeburner, C. Hannah, and R. Beardley (2001), On the geographic and seasonal patterns of the near-surface circulation on Georges Bank-from real and simulated drifters, *Deep Sea Res. Part II*, *48*, 501–518.

Ou, H.-W. (1999), A model of tidal rectification by potential vorticity mixing, part 1: Homogeneous ocean, *J. Phys. Oceanogr.*, *29*, 564–571.

Ou, H.-W. (2000), A model of tidal rectification by potential vorticity mixing, part II: Frontal regime, *J. Phys. Oceanogr.*, *30*, 821–827.

Pietrzak, J. (1998), The use of TVD limiters for forward-in-time upstream-biased advection scheme in ocean modeling, *Mon. Weather Rev.*, *126*, 812–830.

Smolarkiewicz, P. K. (1984), A fully multidimensional positive definite advection transport algorithm with small implicit diffusion, *J. Comput., Phys.*, *54*, 325–362.

Smolarkiewicz, P. K., and T. L. Clark (1986), The multidimensional positive definite advection transport algorithm: Further development and applications, *J. Comput. Phys.*, *67*, 396–438.

Smolarkiewicz, P. K., and W. W. Grabowski (1990), The multidimensional positive definite advection transport algorithm: Nonoscillatory opinion, *J. Comput. Phys.*, *86*, 355–373.

Sukhatme, J., and R. T. Pierrehumbert (2002), Decay of passive scalars under the action of single scale smooth velocity fields in bounded 2D domains: From non self similar pdf's to self similar eigenmodes, *Phys. Rev. E*, *66*, 056302.

D. Chen, R. Houghton, and H.-W. Ou, Lamont-Doherty Earth Observatory, Columbia University, Palisades, NY 10964, USA.

C. Dong, Institute of Geophysics and Planetary Physics, University of California, Los Angeles, 405 Hilgard Ave., Los Angeles, CA 90095, USA. (cdong@atmos.ucla.edu)

T. Ezer, Program in Atmospheric and Oceanic Sciences, Princeton University, Princeton, NJ 08644, USA.